Building and Environment 229 (2023) 109907

Contents lists available at ScienceDirect

Building and Environment

journal homepage: www.elsevier.com/locate/buildenv

Impacts of urban morphometric indices on ventilation

G. Duan [a,c,*], K. Nakamae [b], T. Takemi [b]

[a] Navigation College, Dalian Maritime University, Dalian, PR China
[b] Disaster Prevention Research Institute, Kyoto University, Kyoto, Japan
[c] State Key Laboratory of Coastal and Offshore Engineering, Dalian University of Technology, Dalian, PR China

ARTICLE INFO

Keywords:
Pollutant dispersion
Outdoor ventilation
Tracer age
Urban morphology

ABSTRACT

Ventilation has shown strong sensitivity to urban geometrical heterogeneity; however, the quantitative connection with the urban morphometric indices, e.g. the packing densities (λ_f and λ_p for the frontal and plan area, respectively) and the building-height variability (σ_H), remains unclear. Using large-eddy simulation (LES), the dispersion of a pollutant scalar is investigated for turbulent boundary-layer (TBL) flows developed over real urban regions. While the time history of the domain averaged concentrations follow the familiar exponentially decaying function for all cases, the decay rates differ and there is a clear monotonic dependence on λ_f. The mean tracer age, τ_a, exhibits a strong linear scaling with λ_f as well ($R^2 = 0.8$); however, an unambiguous relationship is hard to be discerned for the ventilation timescales versus the other morphometric indices (e.g. λ_p and σ_H). An effective canyon aspect ratio (AR_{eff}) is proposed for real urban districts, which allows ventilation to be quantified in a simpler manner as that for idealised canyons. The age spectrum, which measures the probability density function of tracer ages across multiple timescales, is analysed to reveal the mechanisms underlying the well-defined connection between ventilation and λ_f. Results are compared with that for an aligned building array of an equivalent canyon aspect ratio to AR_{eff}. The departures reflect the nonlinear effects that are not captured in idealised urban topography setups. The results could be useful for the parameterisation of ventilation in urban areas of complex geometrical profiles and may serve as a reference for urban layout design towards optimum active ventilation capability.

1. Introduction

Urban morphometric features have been significantly modified during the rapid progress of urbanisation [1], leading to district-specific urban microenvironments that differ greatly in the ventilation capability [2,3].

Flow and pollutant dispersion studies for idealised urban geometries have proven an effective probe into the nature of ventilation in realistic urban regions [e.g. 4–7]. A widely used index for the characterisation of urban district geometric properties is the canyon aspect ratio (AR), which is the ratio of the building height over the canyon width. For a 3D building array, the definition applies to both lateral directions. A well known study that successfully related the canyon aspect ratio with the flow properties is the identification of the flow regime transition with respect to AR [8], which was subsequently verified by Hunter et al. [9] using numerical simulation and recently revisited by Ngan and Lo [10] from the perspective of vortex interactions. Ventilation was shown to deteriorate for large AR (deep canyons) and to improve for small AR [11]. However, the canyon aspect ratio that is well defined for idealised canyons may not apply to realistic urban districts, which are heterogeneous in the layout and anisotropic in the building geometrical details [12].

A simple asymmetry of buildings aside a canyon can lead to significant differences in the flow. In the wind-tunnel experiments of Addepalli and Pardyjak [13], a qualitative modification of the flow pattern was observed in a step-up canyon compared to that in a symmetric canyon, suggesting that ventilation pathways would be substantially varied in scenarios of differential geometrical setups. Using numerical modelling, Cui et al. [14] confirmed that ventilation differs greatly in a step-down canyon compared to that in a step-up canyon. It was argued in Gu et al. [15] that uneven building layouts enhance pollutant dispersion in urban canyons. By contrast, a numerical quantification of the influence of urban non-uniformity on ventilation showed that although ventilation improves significantly under a slight increase of the non-uniformity it is likely to deteriorate if the building height variability change is too large [16]. Even for a symmetric urban canyon setup, one with pitched roofs can lead to significant changes in the mean flow and turbulence compared to a flat-roof one [17]. For a more sophisticated geometric setup, Wang et al. [18] and Duan et al. [19]

* Corresponding author at: Navigation College, Dalian Maritime University, Dalian, PR China.
E-mail address: g.duan@my.cityu.edu.hk (G. Duan).

https://doi.org/10.1016/j.buildenv.2022.109907
Received 29 September 2022; Received in revised form 6 December 2022; Accepted 7 December 2022
Available online 17 December 2022

noticed that an elevated walkway overhanging inside a canyon can cause strong perturbations to the turbulent flow around it and lead to qualitatively differing concentration distributions. A strong implication of those results is that there is a high sensitivity of ventilation to urban morphometric features; however, the exact relationship between the two remains unknown.

Characteristic urban morphometric indices that have been popular in the literature include the building packing densities (λ_f and λ_f, the plan- and frontal-area packing densities, respectively), the mean and maximum building heights (H_{ave} and H_{max}, respectively) and the associated building height variability (σ_H) [20]. Urban heterogeneity does not only affect the turbulent flow within the urban canopy but also exerts strong perturbations to higher-level boundary-layer flow through modification of the roughness aerodynamic parameters [21,22]. It was found in Takemi et al. [23] that wind gusts were strengthened under increased building height variability and building arrangement complexity. More conclusive results were obtained in Duan and Takemi [24] for higher-order gustiness statistics, which were shown to scale monotonically with λ_f and λ_p. It was argued therein that σ_H/H_{ave} may serve as a better scaling factor than σ_H. A recent publication in Duan and Takemi [25] illustrated the significant influence of H_{max} on the boundary-layer flow compared to the other indices, which coincides with the results of Kanda et al. [26] and da Silveira et al. [20]. Modified flow pattern and flux exchanges due to varied urban geometrical features contemporarily alters the ventilation routes across the roof-level open boundary.

It is plausible that there exists some conclusive connection between ventilation and the urban morphometric indices, though this has yet remained unclear. Addressing this concern would bring a few obvious benefits. On the theoretical side, identification of the correlation could shed some light on ventilation parameterisation for real urban districts. On the practical side, the results may serve as a useful reference for urban layout design to achieve optimum ventilation capability. Furthermore, understanding the dependence of ventilation timescales on the morphometric indices can be important for policy making and strategy planning during emergency response against accidental releases of hazardous pollutants in urban atmospheric environments.

To reveal the connection between ventilation and urban geometric features, the paper is designed as follows. Section 2.1 describes the morphometric characteristics of 19 real urban districts considered in the current study. In addition to the conventional morphometric indices, an effective canyon aspect ratio, AR_{eff}, is proposed in Section 2.2, which allows the quantification of ventilation versus canyon aspect ratio for real urban districts in a manner similarly to that for idealised canyons. The LES model used for the simulation of pollutant dispersion is briefly described in Section 2.3. Mathematical definition and physical interpretation of the tracer age statistics are introduced in Section 2.4. Besides the scalar decay (Section 3.1) and the mean tracer age distribution (Section 3.2), the scaling of characteristic ventilation timescales with AR_{eff} is quantified in Section 3.3. Section 3.4 analyses the age spectra, wherein a comparison is made with respect to results obtained for an aligned building array. Summary and discussion are given in Section 4.

2. Methodology

2.1. Morphometric features of the urban districts

The urban districts considered in the current study are from a few real urban areas in Japan. They differ in the morphometric features, which include the frontal- and plan-area packing densities (λ_f and λ_p, respectively), the mean and maximum building heights (H_{ave} and H_{max}, respectively), and the building-height variability (σ_H).

Some surface texture characteristics are presented in Fig. 1 with the morphometric statistics indicated on the top of each plot. They consist of densely-packed ($\lambda_p = 0.79$) but low H_{ave} districts, such as panel a (Kyoto centre); a mediumly-packed area ($\lambda_p = 0.43$) filled with a huge portion of irregularly-shaped and arranged building obstacles, panel b (Yamashina, an area located in the East of Kyoto City); also densely-pack but high H_{ave} districts, such as panel c (Namba, a business district located in the South of Osaka) and panel d (around Osaka station), which are representative of typical high-density commercial land uses; medium-density ($\lambda_p = 0.51$) areas containing a group of skyscrapers (H_{max} as high as 189 m), such as panel e (Temma), a neighbourhood in the East of Osaka; and sparsely-packed areas ($\lambda_p = 0.34$), such as panel f, which is also located in Temma and may represent scattered pocket urban areas surrounding commercial regions. Obviously, the districts also differ greatly in σ_H and λ_f. The λ_p range herein is broader than that considered in Liu et al. [27].

Table 1
Domain dimension and value ranges of the morphometric indices. The spatial resolution in the streamwise (x), spanwise (y) and vertical (z) is isotropic for $z < 80$ m, i.e. $\Delta x = \Delta y = \Delta z = 2$ m. For $z \geq 80$ m, Δz is vertically stretched with a factor of 1.08 until $\Delta z \geq 16$ m, yielding a domain height of $L_z \approx 490$ m.

H_{ave} (m)	H_{max} (m)	σ_H (m)	λ_p	λ_f	$L_x/\Delta x$	$L_y/\Delta y$
[8, 31]	[36, 189]	[4, 33]	[0.34, 0.79]	[0.25, 0.85]	336	272

In total, 19 cases are examined for the purpose of covering a range of the morphometric features as wide as possible. Statistics of the morphometric indices and the domain dimensions are summarised in Table 1. The range of the indices are roughly consistent with that investigated in [23] and comparable with the European cities (London, Toulouse and Berlin), but disparate from the North American city, Los Angeles, which has buildings sparsely and evenly distributed but has a large portion of skyscrapers with H_{ave} as high as 51 m [28].

2.2. Effective canyon aspect ratio, AR_{eff}

In addition to the conventional morphometric indices, we propose an effective canyon aspect ratio, $H_{\text{ave}}/W_{\text{ave}}$, which enables the characterisation of the canyon geometric feature for realistic urban districts in a convenient manner as that for idealised canyons. Herein, W_{ave} denotes the mean canyon width; however, unlike the mean building height (H_{ave}) the calculation of W_{ave} is not straightforward for an inhomogeneous urban area, wherein the canyons are unevenly distributed and the building obstacles are anisotropic in 3D details [12].

An alternative to W_{ave}, hereafter denoted as W_{eff}, may be achieved by conceiving a nominal domain (see Fig. 2 for a schematic illustration), wherein the alignment of the cubic building blocks mounted on the ground is assumed homogeneous, but the lateral dimensions (L_x and L_y) and the packing densities (λ_p and λ_f) are kept the same as that for the associated realistic urban district. Rearranging the familiar formulae for the frontal- and plan-area packing densities,

$$\lambda_p A_T = A_p = W_{\text{eff}}^2 \quad \text{and} \quad \lambda_f A_T = A_f = W_{\text{eff}} H_{\text{ave}}, \tag{1}$$

where A_f denotes the frontal area (the vertical area facing the approaching wind), A_p denotes the roof (or plan) area, and A_T is the lot area associated with each building obstacle. Manipulation of Eq. (1) yields

$$W_{\text{eff}} = \frac{H_{\text{ave}} \lambda_p}{\lambda_f}, \tag{2}$$

which represents an effective mean canyon width for the realistic urban district in question. The canyon aspect ratio immediately follows

$$AR_{\text{eff}} \equiv \frac{H_{\text{ave}}}{W_{\text{eff}}} = \frac{\lambda_f}{\lambda_p}, \tag{3}$$

which is referred as the effective canyon aspect ratio for a realistic urban. Herein, $AR_{\text{eff}} = [0.46, 1.65]$.

By definition, the breadth involved in the calculation of λ_f for a real urban district depends on the wind direction [29]; however, one can always require a perpendicular wind to the frontal building facade of the nominal array for the realistic district of concern (as ketched in Fig. 3), without impeding equivalent λ_f and λ_p from being retained.

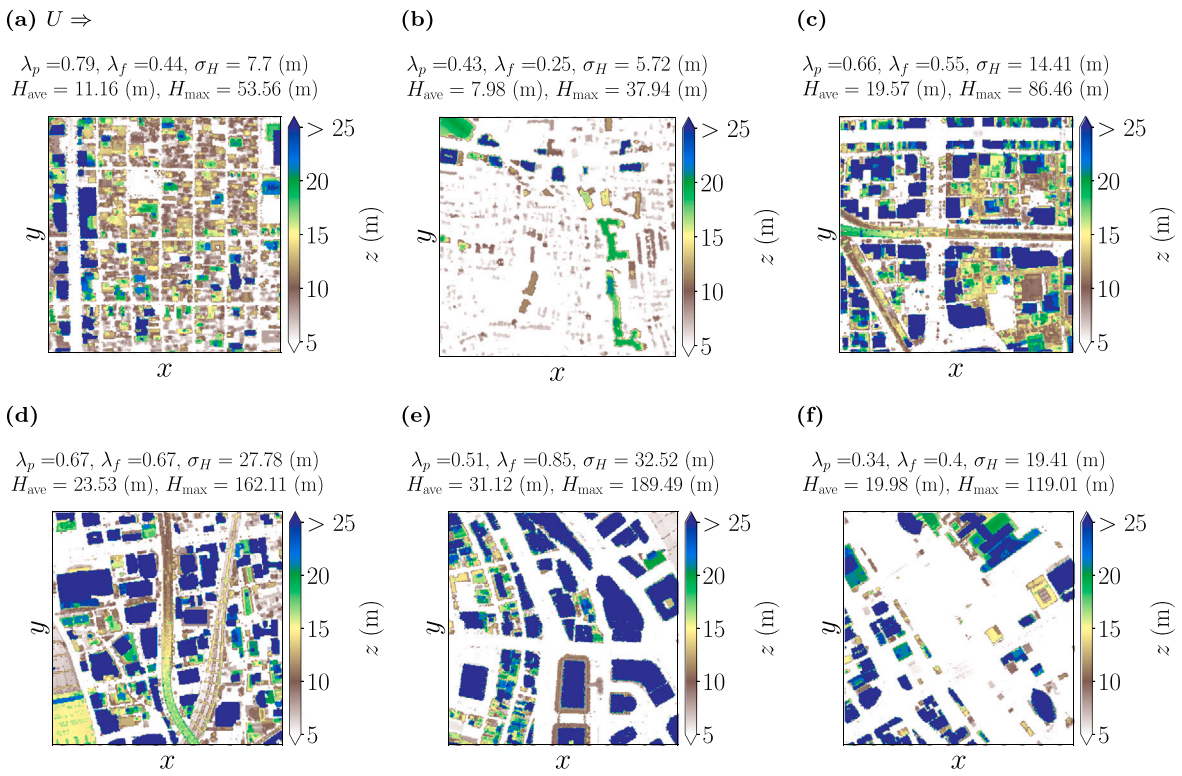

Fig. 1. Real urban districts in Japan: (a) Kyoto centre; (b) Yamashina; (c) Namba; (d) Osaka station; (e,f) Temma. Plots are shaded by the building heights. Lateral dimensions of the squared areas are $L_x \times L_y$=500 m×500 m. Statistics of the morphometric indices (λ_p, λ_f, σ_H, H_{ave} and H_{max}) are indicated on the top of each plot and summarised in Table 1 for all the 19 cases. A buffer area filled with cubical blocks surrounding the urban region is excluded in the plot for brevity. The arrow in the figure caption to panel a indicates the primary wind direction, for which λ_f is evaluated.

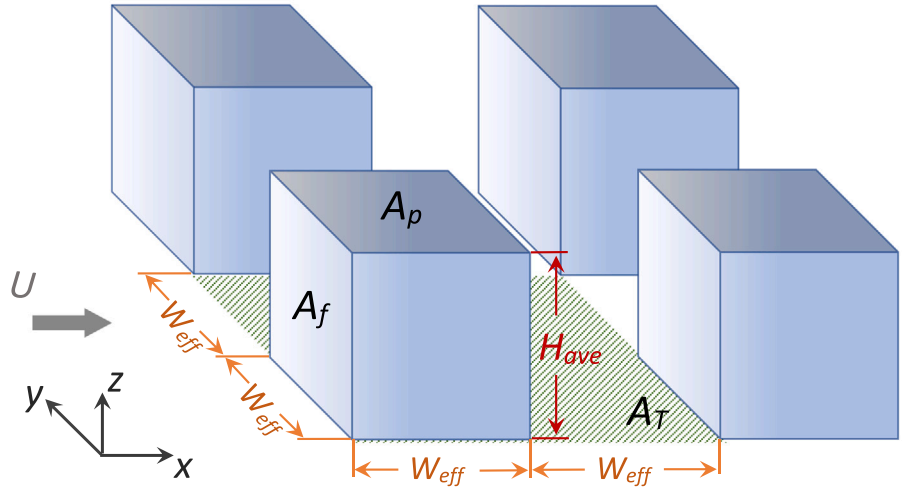

Fig. 2. Schematic diagram of one unit element (with the lot area, A_T, shaded in green) of the nominal domain for a realistic urban district of the same λ_f, λ_p, H_{ave} and lateral dimensions (L_x and L_y). W_{eff} denotes an effective mean canyon width associated with the realistic urban district.
Source: Plot readapted after Grimmond and Oke [21].

2.3. Numerical experiments

2.3.1. Large-eddy simulation

The building-resolving LES model, PALM 6.0 [30], is used to simulate the turbulent boundary-layer flow and pollutant dispersion. PALM was originally developed at the Institute of Meteorology and Climatology of Leibniz Universität Hannover, Germany [31] and specifically designed for atmospheric and oceanic boundary layer flows. It is based on the implicitly filtered non-hydrostatic and incompressible Navier–Stokes equations in Boussinesq-approximated form. Details of the governing equations can be found in Maronga et al. [30].

2.3.2. Pollutant source and pseudo large-scale forcing

Similarly to Duan and Ngan [7], a ground-level 'line' source, S, prescribed at $\vec{x}_0$ (wherein $x = [4l, 5l]$ upstream of the urban area and $y = [0, L_y]$), is released at an initial instant, t_0, as an impulse after the flow has reached statistically steady state, viz.

$$S = C_0 \delta(t - t_0, x - \vec{x}_0), \tag{4}$$

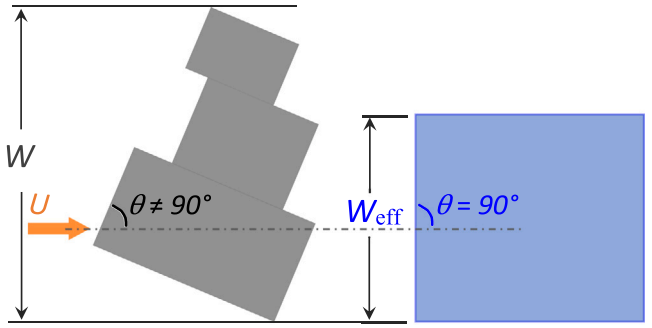

Fig. 3. The region shaded in grey represents an area occupied by a building obstacle of a realistic urban district. The breadth, W (so does λ_f), depends on the wind direction, θ. The squared area shaded in blue denotes an idealised building cuboid, which belongs to a nominal building-array that requires a perpendicular wind but the same λ_f, λ_p, H_{ave} and lateral dimensions (L_x and L_y) as the real urban district in question. (For interpretation of the references to colour in this figure legend, the reader is referred to the web version of this article.)

where C_0 is the source strength and is specified arbitrarily as in Duan et al. [32], l denotes the lateral dimensions of the roughness cuboids in the buffer region surrounding the urban area and is fixed at 10 m similarly to the setting in Yoshida et al. [33]. Following Duan and Takemi [24], the height of the roughness elements is equal to the mean building height, H_{ave}, associated with each urban district. A buffer area filled with cubic roughness elements has been adopted in the literature as a common practice for diminishing the influence of building-height discontinuity, which might arise in particular due to the (spanwise) periodic boundary condition, e.g. Park et al. [34].

The construction of the initial-value problem allows the calculation of the tracer age statistics (see Section 2.4), which will be used as diagnostics for ventilation (see Section 3.2).

As in Lo and Ngan [35] and Furtak-Cole and Ngan [36], the dispersion of pollutants is driven by a turbulent boundary-layer flow, U, through turbulence recycling [37,38], whereby turbulence, $u_i'(y,z,t)$, extracted every time step at a recycling plane, x_{rec}, near the outflow is fed back to the inflow boundary and superimposed on a temporally- ($\overline{\cdot}$) and horizontally-averaged ($\langle\cdot\rangle$) wind profile, $\langle\overline{u_i}_{,pre}\rangle(z)$, obtained from statistically steady-state data of a precursor run. Formally,

$$U = \langle\overline{u_i}_{,pre}\rangle(z) + u_i'(y,z,t), \tag{5}$$

where $\langle\overline{u_i}_{,pre}\rangle(z)$ of the precursor run is forced by a specified pressure gradient, $\Delta P = 0.6\times10^{-3}\,\mathrm{Pa\,m^{-1}}$, with periodic lateral boundary conditions.

The inflow wind, U, mimics a pseudo external large-scale forcing, which yields a moderate to high Reynolds number TBL flow, $Re \equiv U_\infty H_{ave}/\nu = \mathcal{O}(10^6) - \mathcal{O}(10^7)$ based on H_{ave} and $U_\infty \sim 4.7 - 8.4\,\mathrm{m\,s^{-1}}$ (the horizontally averaged freestream wind speed). The TBL flows considered herein are comparable to that studied in Hertwig et al. [39] and Horiguchi et al. [40] for realistic urban topographies and in Duan and Ngan [7] for an aligned building array.

2.3.3. Boundary conditions and numerical schemes

A Prandtl layer is assumed between the roughness height ($z_{0,m} = 0.1$ m for momentum, as in Park et al. [34]) and the first grid level, whereby the Reynolds shear stresses are parameterised following the Monin–Obukhov similarity theory [41]. The roughness height for passive scalar is the same as $z_{0,m}$. Unresolved subgrid-scale (SGS) turbulent fluxes are parameterised using the modified 1.5-order Deardorff closure [42]. SGS eddy diffusivities are obtained by solving a prognostic equation for the SGS turbulent kinetic energy (SGS-TKE). As in Duan et al. [19], the turbulent Schmidt number is unity.

In the streamwise (x), non-cyclic boundary conditions are applied, namely there is Dirichlet at the inlet and radiation at outlet, in combination with turbulence recycling described in the above section. In the spanwise (y), periodic boundary conditions are used. At solid surfaces, there is no-slip for the velocity components and Neumann for scalars. Neumann boundary conditions are also applied at the domain top.

As summarised in Table 1, the spatial resolution is isotropic for $z < 80$ m, namely the grid spacings in the streamwise (x), spanwise (y) and vertical (z) are the same, $\Delta x = \Delta y = \Delta z = 2$ m. The resolution has proven adequate for resolving urban boundary-layer turbulence [e.g. 33,43]. For the higher part of the domain ($z \geq 80$ m), wherein energy is increasingly possessed by larger scales [44], Δz is vertically stretched with a stretching factor of 1.08 until $\Delta z \geq 16$ m while Δx and Δy remain equidistant so as to prevent over grid deformation [25]. This discretisation ensures model accuracy with acceptable computing power. A third-order Runge–Kutta time-stepping scheme [45] and a fifth-order finite differencing scheme [46] are used to solve the advection terms in the conservation equations. The Poisson equation for the modified perturbation pressure resulting from the predictor–corrector method [e.g. 47] is solved with an iterative multigrid method, which does not require periodicity along the horizontal directions [48].

Data are collected with a temporal resolution of $\Delta t = 10$ s and analysed for the last 3600 s, after a spin up of $t_f = 6$ h, whence the flow are statistically steady. Therefore, $t_f - t_0 = 3600$ s.

2.3.4. Model validation

Validation of the wind profiles and second-order turbulence statistics can be found in many previous studies of urban turbulent boundary-layer flows for idealised canyons [e.g. 49–51] and realistic urban districts [52] using the same LES model. Since the current work is focused on the passive scalar, the validation presents comparison of the scalar statistics against measured data.

A ground-level line source is set along the centreline of a unit-aspect-ratio street canyon, identical to the configuration in the wind-tunnel measurements of Pavageau and Schatzmann [53]. Because comparison of the mean concentration profiles near the leeward, windward and at the canyon centreline has been performed in Duan et al. [32] and the concentration fields in Lo and Ngan [16], which show reasonably good agreement with the experimental data, it is not repeated here. The current validation examines the second-order scalar statistics. Although they cannot be expected to have an agreement with the measurements as good as that for the mean profiles, Fig. 4 shows that the overall pattern of the nondimensionalised variances of the concentration fluctuations, $\left\langle \sqrt{\overline{C'^2}}/\overline{C} \right\rangle$ (where angle brackets and overbar denote respectively the spanwise and time averages) is qualitatively close to the wind-tunnel data. Comparable discrepancies are seen as well in the validation of LES model in Liu and Barth [54].

2.4. Tracer age statistics and notation

The tracer age statistics include the age spectrum and the mean tracer age (MTA) [55]. The former describes the probability density function of the ages, $\xi \equiv t - t_0$, connecting a tracer at a source location of $\vec{x}_0$ to the arrival at a receptor, $\vec{x}$. The latter is simply the first moment of the age spectrum, and therefore quantifies the average time for a pollutant parcel to travel from $\vec{x}_0$ to $\vec{x}$. Small MTA implies improved ventilation.

Formally, the age spectrum can be obtained from the Green's function, $G(\vec{x},\xi|\vec{x}_0,t_0)$, which is simply the solution to the advection–diffusion equation for the delta-function source (Eq. (4)),

$$Z(\vec{x},\xi|S) = \frac{\int_D d\vec{x}_0 G(\vec{x},\xi|\vec{x}_0,t_0)S(\vec{x}_0)}{C(\vec{x},t)}, \tag{6}$$

where $\xi = t - t_0$. The mean tracer age then reads

$$\tau_a(\vec{x}) = \int_0^{t_f-t_0} \xi Z(\vec{x},\xi|S)d\xi, \tag{7}$$

where $t_f - t_0 = 3600$ s as described in Section 2.3.3 and D in the integration term denotes the entire domain.

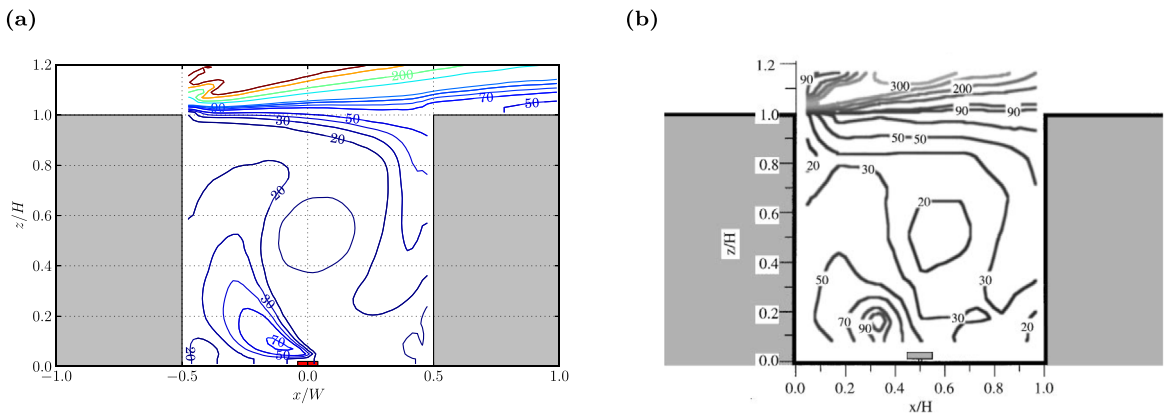

Fig. 4. Comparison of the turbulence intensity of the scalar field inside and above the canyon, $\left\langle \sqrt{\overline{C'^2}}/\overline{C} \right\rangle$. (**a**) Current LES; (**b**) wind-tunnel data from Pavageau and Schatzmann [53].

Application of the MTA concept was initially explored in the urban air quality literature in Lo and Ngan [16], wherein derivations are more comprehensively presented. Merits of the age spectrum and associated mean tracer age in comparison with other ventilation diagnostics [e.g. 56,57] are discussed therein as well. Formulas of higher-order moments associated with the age spectrum (e.g. standard deviation and kurtosis) can be found therein as well. The MTA has proven a convenient timescale diagnostic for the unsteadiness of ventilation in urban flows in a series of subsequently published studies [e.g. 7,58].

With no confusion with the angle brackets defined in the previous text (e.g. in Eq. (5)), hereafter $\langle\cdot\rangle$ denotes that quantity is spatially averaged in the vertical. Domain average is denoted with a caret (or "hat"), $\hat{(\cdot)}$.

3. Results

3.1. Scalar decay

Fig. 5 plots the decay of the domain averaged concentrations, $\hat{C}/C_0$, for various λ_f. It can be seen the decay is exponentially fast, which agrees with previous studies [32,59]. It is found in the current study that the decay rate, $d(\hat{C}/C_0)/dt$, slows down progressively towards higher λ_f; however, the dependence of $d(\hat{C}/C_0)/dt$ on the other urban morphometric indices is not conclusive, except that for H_{ave}, which is unsurprising because H_{ave} is directly involved in the definition of λ_f. Normally, one would compare averages within the canyons; however, H_{ave} differs for real urban districts. It is therefore more suitable to consider domain averaging instead of canyon averaging.

Intuitively, one expects improved ventilation for high σ_H; however, a clear scaling of the ventilation timescales with σ_H is not identified. This actually coincides with the finding of Lo and Ngan [16] that a minor increase of the urban non-uniformity (namely σ_H) may enhance ventilation significantly (the mean tracer decrease was shown to be up to ~50%) but a large change of σ_H does not necessarily guarantee improved ventilation.

The reason for the well defined dependence of pollutant decay on the frontal area packing density, λ_f, is presumably because λ_f affects the pollutant dispersion in a more direct manner. It was shown in Duan and Ngan [7] that ventilation across the lateral boundaries of an idealised building array changes more rapidly than through the roof level. It can be seen from the schematic illustration in Fig. 6 that an increase in the frontal area is associated with increasing building height (H) or breadth (W). The former yields a deeper canyon (panel a); the latter leads to a narrowing of the street width (panel b). Ventilation pathways through the street channels (or channelling) get squeezed in both scenarios, which effectively slows down the decay of pollutants in the control domain. By contrast, it is not obvious that the rapidity of the scalar decay should scale monotonically with the other morphometric indices.

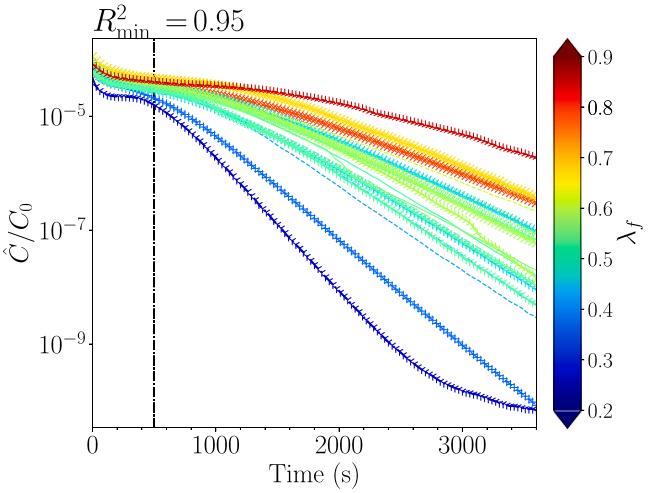

Fig. 5. Scalar decay of the domain averaged concentrations, $\hat{C}/C_0$, for different λ_f.

For realistic urban districts and meteorological conditions, the orthogonality of the primary wind direction and the building facades confronting the approaching wind are not necessarily ensured; however, as postulated in Section 2.2 that one can always conceive a nominal facade, A_f, that is perpendicular to the approaching wind (cf. Fig. 3). A modified λ_f due to changing wind directions directly implies changes in the breadth or height associated with A_f. An increase in λ_f naturally leads to the narrowing of street channels. It is therefore argued that the above rationale holds for varying wind directions.

Fig. 7 plots the decay timescales, τ_r, also known as the retention time (DePaul and Sheih [59]), viz.

$$\hat{C}/C_0 \sim \exp(-\frac{t}{\tau_r}), \tag{8}$$

for different λ_f. There is notably a strong linear scaling of τ_r with λ_f ($R^2 \sim 0.76$). The initial spin up ($T_{\text{spin}} = 500\,\text{s}$) and the late-stage attenuation are excluded in the least squares regression of the decay profiles (Fig. 5). The standard deviation of τ_r, $SD[\tau]$, for each decay lies within the range of $SD[\tau] = [0.5, 15]\,\text{s}$. Like [32], SD is propagated from the error of the decay slope, λ, i.e. $SD[\tau] = SD[1/\lambda] \approx 1/E[\lambda]^2 \times SD[\lambda]$, where E denotes the expectation operator.

Unlike an idealised street canyon, for which a well-defined T_{spin} can be conveniently calculated, an accurate estimation of T_{spin} can be

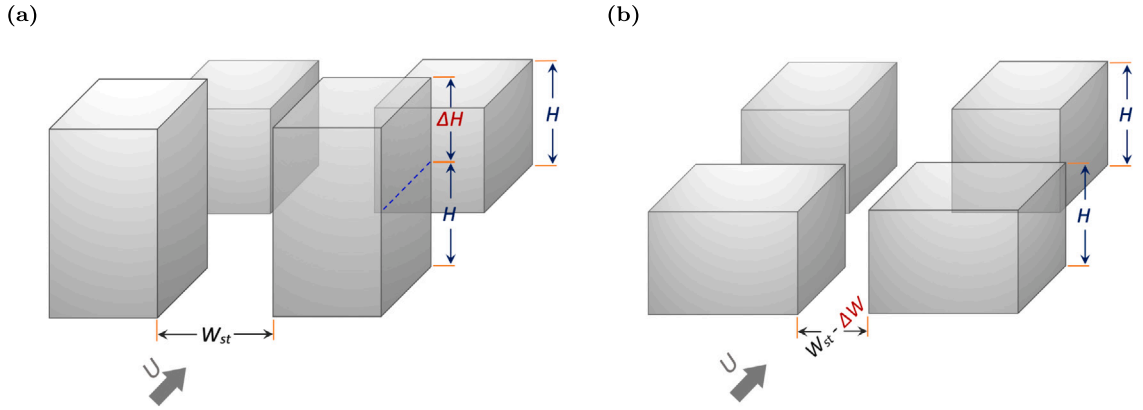

Fig. 6. Sketched squeezing of ventilation pathways through the street channels for increased λ_f.

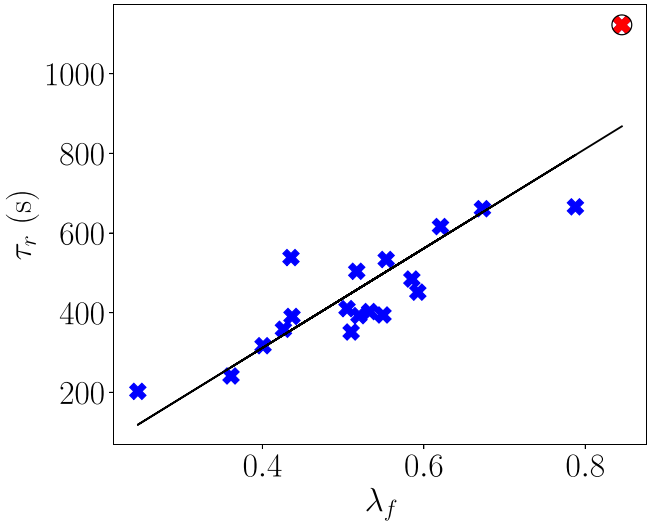

Fig. 7. Decay timescales (or retention times, Eq. (8)), τ_r, of the domain averaged concentrations, $\hat{C}/C_0$, versus λ_f. The solid line corresponds to a least-squares fit and the scaling follows $\tau = 1249\lambda_f - 188$ with $R^2 \sim 0.76$. The circled cross marker coloured in red indicates the case of the largest discrepancy, which is identified to occur for the urban district with a skyscraper of $H_{\max} = 189$ m (see Fig. 1e). (For interpretation of the references to colour in this figure legend, the reader is referred to the web version of this article.)

hard for realistic urban districts. The spin up time herein follows the suggestion of Duan and Ngan [51] that T_{spin} is comparable to the eddy turnover timescale, τ_{eddy}, which roughly quantifies the timescale for a pollutant scalar to be advected from the ground to the canyon roof. The calculation of τ_{eddy} for a real urban region will be discussed in Section 3.3.1.

3.2. Mean tracer age

Fig. 8 plots the MTA distributions for a few urban regions considered in the current study. Counterintuitively, ventilation deteriorates (high $\hat{\tau}_a$) in sparsely-packed areas (for example, panel e) in comparison to that in densely-packed regions (in particular panel a, for which the plan area building packing density, λ_p, is as high as 0.79), indicating that a clear relationship of $\hat{\tau}_a$ versus λ_p may not be easily identifiable. By contrast, ventilation seems to improve (low $\hat{\tau}_a$) in areas of small λ_f (e.g. panel a) and to deteriorate for large λ_f (e.g. panel e).

The difference between impacts of λ_f and λ_p on MTA is likely because they quantify essentially differential geometrical aspects of real urban districts. Although they both have influences on the ventilation, the former can be of importance for "two-way" ventilation (i.e. ventilation through the street channels and across the roof-level open boundary—because the building-heigh change can effectively deepen or widen a canyon, as sketched in Fig. 6) whilst the latter may be only influential in "one-way" ventilation (i.e. pollutant removal from street channels, because building height is not involved in the definition of λ_p). The result coincides with the pollutant decay (discussed in Section 3.1), wherein λ_f exhibits a more distinguishable monotonic impact on the decay rate.

Fig. 9 confirms the strong linear scaling of the domain-averaged MTA, $\hat{\tau}_a$, with λ_f. It is found that a scaled λ_f, $\lambda_{f,\text{eff}} \equiv \lambda_f H_{\text{ave}}/\sigma_H$ (an effective λ_f firstly proposed in the study of urban wind gustiness in Duan and Takemi [24]), does not change the scaling qualitatively—the R^2 for $\hat{\tau}_a$ versus $\lambda_{f,\text{eff}}$ is as high as 0.76 (plot now shown), implying that H_{ave}/σ_H may only function as a coefficient in the scaling. However, a strong linear scaling is also seen for $\hat{\tau}_a$ versus H_{ave} ($R^2 \sim 0.71$, see Fig. 10), which is directly proportional to λ_f. The largest discrepancies in both plots are likely attributable to perturbations of notably tall buildings: $H_{\max} = 113$ m for the former and $H_{\max} = 120$ m for the latter (cf. Table 1). The $H_{\max}/H_{\text{ave}}$ is up to 7. Similar results are also found in the following sections (see Table 2 in Sections 3.3.1–3.3.2).

It is noteworthy that the correlation of ventilation (herein characterised using $\hat{\tau}_a$) with the urban topographical indices needs to be interpreted with caution in certain scenarios. A typical example is the setup of a point source, for which the polluted area strongly depends on the forcing; namely, a pollutant scalar may not reach buildings and canyons far outside the plume edge (cf. Kanda and Yamao [60]). In the current work, an upstream line source (which has a same spanwise dimension as the control domain) essentially takes into account the influence of all building obstacles on the scalar dispersion. Since the topographical indices are evaluated for the entire domain of each LES, a line source appears more suitable for the purpose of the current work compared to a point source or an area source prescribed for a subset surface inside an urban region, e.g. Boppana et al. [5].

3.3. Scaling of characteristic timescales with AR_{eff}

3.3.1. Eddy turnover timescale, τ_{eddy}

Unlike the tracer age, which directly evaluates the temporal evolution of a tracer parcel (Section 3.2), an eddy turnover timescale, τ_{eddy}, quantifies the time taken for a fluid parcel to be advected from the ground to the roof-level open boundary [7]. For an idealised urban canyon, wherein closed streamlines are well defined, τ_{eddy} can be approximated by the mean circulation timescale [61], viz.

$$T_c \equiv 2\left(\frac{W}{U_{\text{rms}}} + \frac{H}{W_{\text{rms}}}\right) \quad \text{or} \quad T_1 \equiv 2\left(\frac{W}{U_1} + \frac{H}{W_1}\right), \tag{9}$$

where U_{rms} and W_{rms} are spatially averaged root-mean-square streamwise and vertical velocities within the canyons, and U_1 and W_1 denote

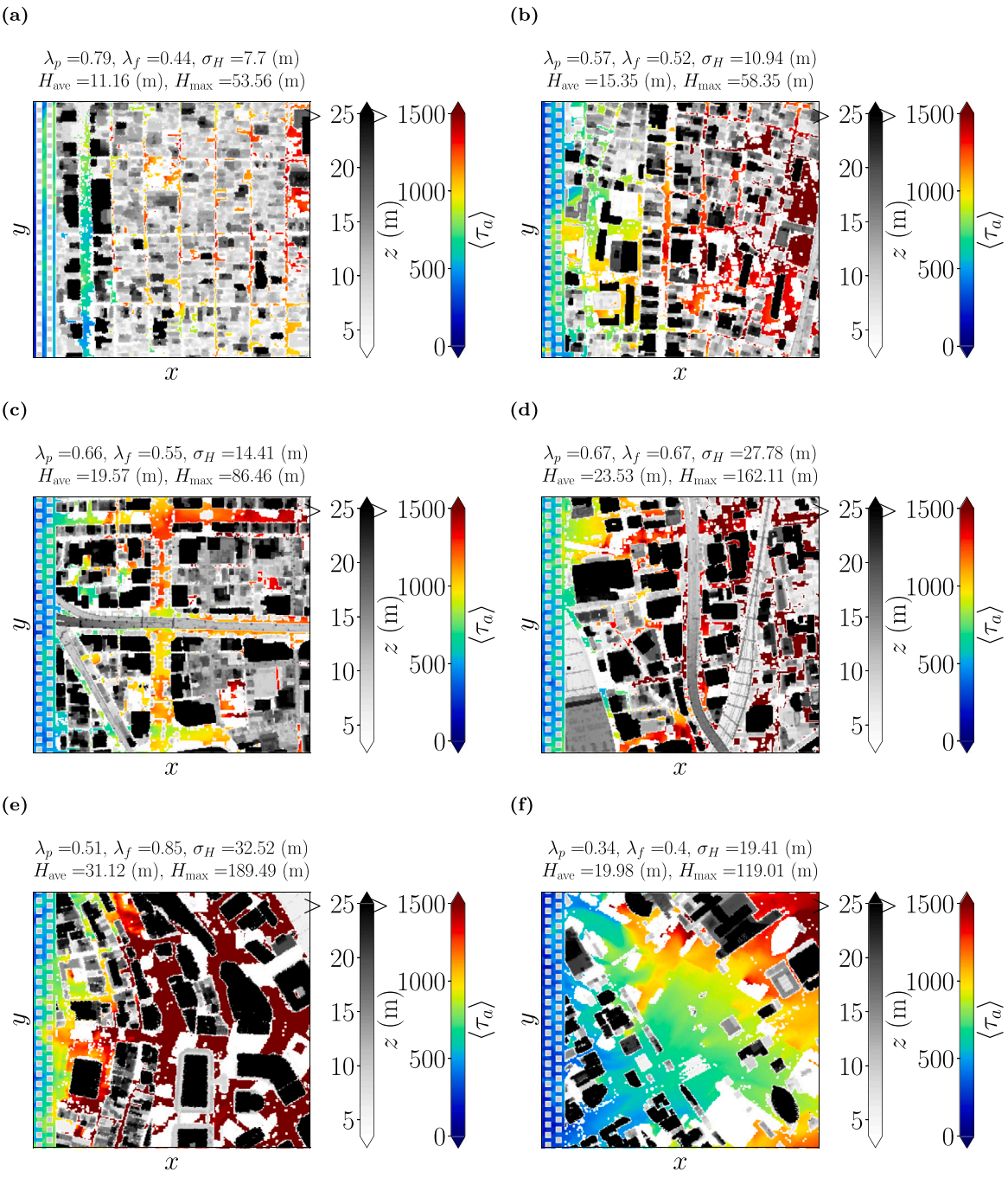

Fig. 8. Distribution of vertically averaged MTA, $\langle \tau_a \rangle$, for Kyoto centre (panel a), Namba (panels b, c), Osaka station (panel d) and Temma (panels e, f). The colour map in grey scale indicates the building heights and the colourful one indicates $\langle \tau_a \rangle$. The upstream roughness elements are shown for clarity of the source location at $x = [4l, 5l]$ and $y = [0, L_y]$, where l denotes the lateral dimensions of the cuboids (see Section 2.3.2) and L_y is the spanwise dimension of the domain (see Table 1). (For interpretation of the references to colour in this figure legend, the reader is referred to the web version of this article.)

spatial averages of the absolute values of the associated velocity components. However, T_c and T_1 may be less appropriate for realistic urban topographies because they tacitly assume a well-defined central vortex that is inscribed within the canyon.

An alternative characteristic velocity in place of the root-mean-square or the absolute-value velocities is therefore needed for the calculation of τ_{eddy}. Given that a well-defined logarithmic layer can develop despite idealised [62] or realistic [25] urban topographies, it is suggestive that the friction velocity, u_* (which is associated with the aerodynamic characteristics of an urban boundary-layer flow), may be used instead. Although u_* is derived from the wind profile above the roughness sublayer, it is essentially a scaling parameter that characterises the dynamics inside the canopy, specifically the momentum exchanges, which are driven by the eddy circulation, between the canopy and the atmosphere aloft. The eddy turnover timescale then reads

$$\tau_{eddy} \equiv \frac{H_{ave}}{u_*}, \tag{10}$$

where u_* is calculated using the Levenberg–Marquardt (LM) algorithm to minimise the squared departure of simulated wind profile within the logarithmic layer and the log-law function. An application of the LM algorithm in regression of the urban surface roughness aerodynamic parameters can be found in Duan and Takemi [25].

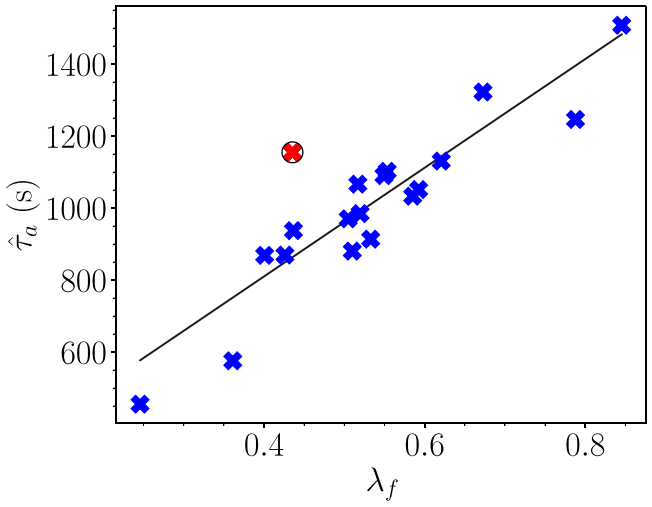

Fig. 9. MTA, $\hat{\tau}_a$, versus the frontal area building packing density, λ_f. The solid line corresponds to a least-squares fit and $R^2 = 0.80$. The circled cross marker coloured in red indicates the case of the largest discrepancy, which is identified to occur for the urban district with notably tall buildings ($H_{max} = 113$ m). (For interpretation of the references to colour in this figure legend, the reader is referred to the web version of this article.)

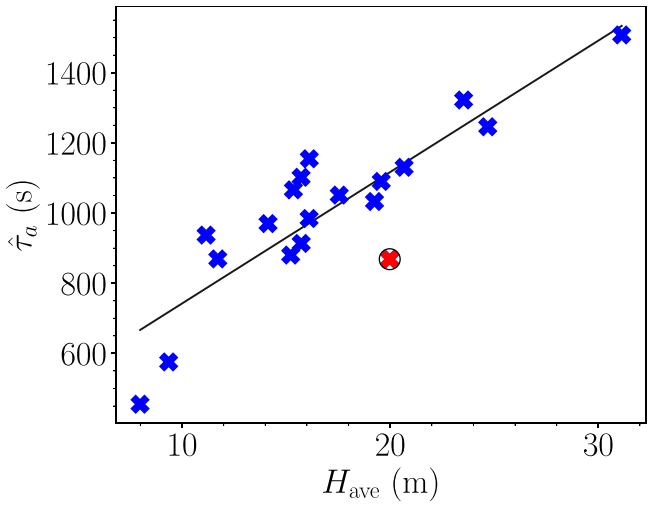

Fig. 10. As in Fig. 9, but for $\hat{\tau}_a$ versus the mean building height, H_{ave}, and $R^2 = 0.71$. The circled cross marker coloured in red indicates the case of $H_{max} = 120$ m (see Fig. 1f). (For interpretation of the references to colour in this figure legend, the reader is referred to the web version of this article.)

As shown in Fig. 11, τ_{eddy} is large in 'deep canyons', implying that longer time is required for a fluid parcel to be swept from the ground to the roof, which is in agreement with observations [e.g. 63]. The largest departure from the quadratic fit occurs for $H_{max} = 170$ m, which is close to the maximum building height (~180 m) in Kowloon Peninsula, a highly-densely-packed urban area in Hong Kong (Yao et al. [64]).

3.3.2. Ventilation timescales, τ_r and τ_a

The proposed effective canyon aspect ratio, AR_{eff}, for realistic urban topographies also allows to quantify the scaling of the ventilation timescales (herein the retention time, τ_r, discussed in Section 3.1 and the mean tracer age, $\hat{\tau}_a$, analysed in Section 3.2) with AR_{eff}. Although similar studies are seen in published work [e.g. 7,58], the main focus was on idealised urban setups. Attempts for realistic urban districts have been scarcely made.

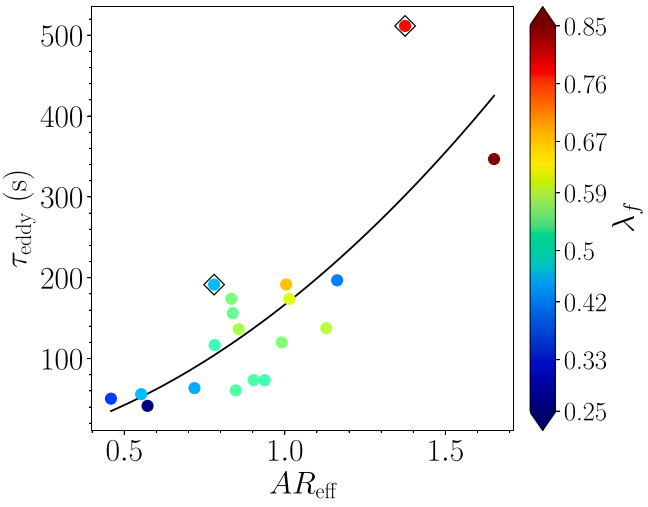

Fig. 11. Eddy turnover timescale, τ_{eddy}, versus the effective canyon aspect ratio, AR_{eff}. The quadratic regression (solid line) is plotted for reference ($R^2 = 0.64$). The scattered values are shaded by λ_f for reference. The squared circles indicate cases of the largest and the second largest departures from the fitting curve.

Table 2
Summary of the morphometric indices associated with cases that exhibit the largest and the second largest departures from the fitting curves in Fig. 11 for τ_{eddy} versus AR_{eff}, and Fig. 12 for τ_r versus AR_{eff} (panel a) and $\hat{\tau}_a$ versus AR_{eff} (panel b). For most of them, H_{max} is shown to be high.

Topography indices	H_{max} (m)	σ_H (m)	H_{ave} (m)	λ_p
Revisit Table 1	[36, 189]	[4, 33]	[8, 31]	[0.34, 0.79]
AR_{eff} vs τ_{eddy} (Fig. 11)	**119** (Fig. 1f), 38 (Fig. 1b)	19, 6	20, 8	0.34, 0.43
AR_{eff} vs τ_r (Fig. 12a)	**170**, **113**	21, 15	25, 16	0.57, 0.56
AR_{eff} vs $\hat{\tau}_a$ (Fig. 12b)	**119** Fig. 1(f), **162** (Fig. 1d)	19, 28	20, 24	0.34, 0.67

It can be seen in Fig. 12 that ventilation deteriorates (corresponding to large ventilation timescales) when AR_{eff} is increased, which coincides with results of idealised 2D street canyons [4,11].

Cases that show notably large departures from the fitting curves are identified to contain exceptionally tall buildings, as summarised in Table 2. According to the λ_p column, this can occur in both sparsely-packed ($\lambda_p = 0.34$) and densely-packed urban regions ($\lambda_p = 0.67$). Although a comparably high displacement from the regressed curve is also seen for a low H_{max} case (see the value corresponding to Fig. 11 in the second column of H_{max}), it is confirmed that this area is filled with a huge portion of irregularly shaped building obstacles (plot now shown). While clarification of the quantitative influence of skyscrapers on ventilation timescales requires more efforts, the current results suggest that H_{max} may serve as an important factor for further improving the parameterisation. A similar highlight was reported in previous studies [25,26,65]. Although they were concerned about the parameterisation of urban surface roughness aerodynamic parameters, it is plausible that the exact influence arises from the urban canopy height that is dynamically modulated by the exceptionally tall buildings (Cheng and Yang [66]).

3.4. Age spectrum

The physical mechanisms underlying the dependence of the ventilation timescales on the urban morphometric indices (specifically AR_{eff} and λ_f) analysed in the previous sections may be elucidated from the tracer age spectra. As introduced in Section 2.4, age spectrum describes the statistical distribution of the tracer ages connecting the source and the receptor, and characterises the unsteady processes involved in ventilation. It is reasonable to expect that any change in the geometrical

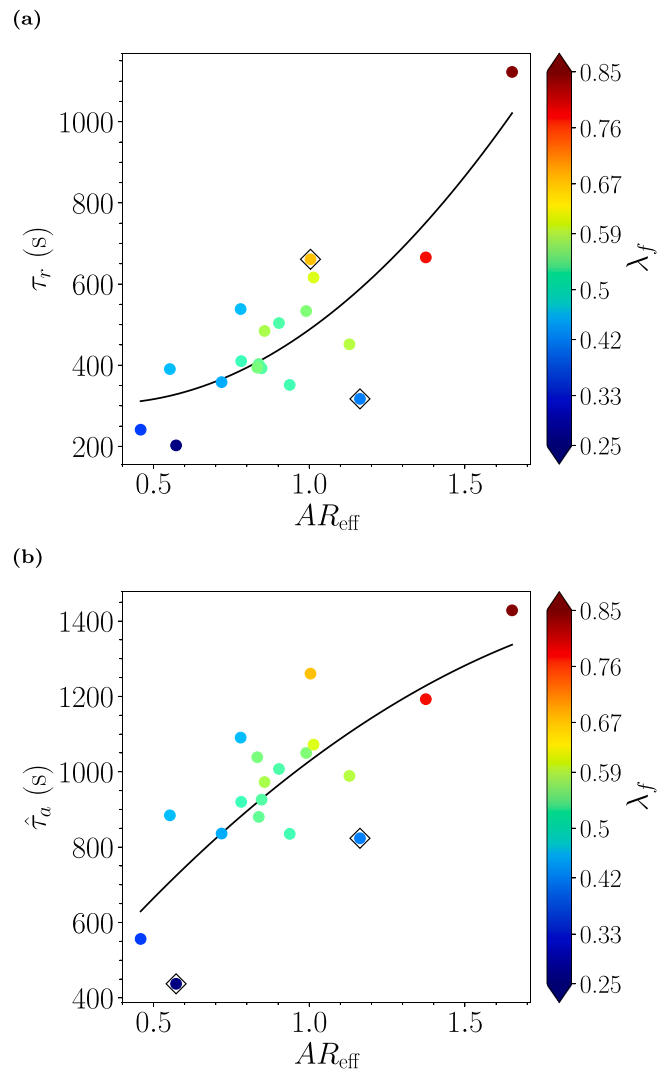

Fig. 12. Retention time, τ_r, versus AR_{eff}; (b) MTA, $\hat{\tau}_a$, versus AR_{eff}. As in Fig. 11, solid lines denote the quadratic regression ($R^2 = 0.59$ for results in panel a and $R^2 = 0.70$ for panel b). Cases that exhibit the maximum and the second largest departures from the fitting curves are annotated using squared circles.

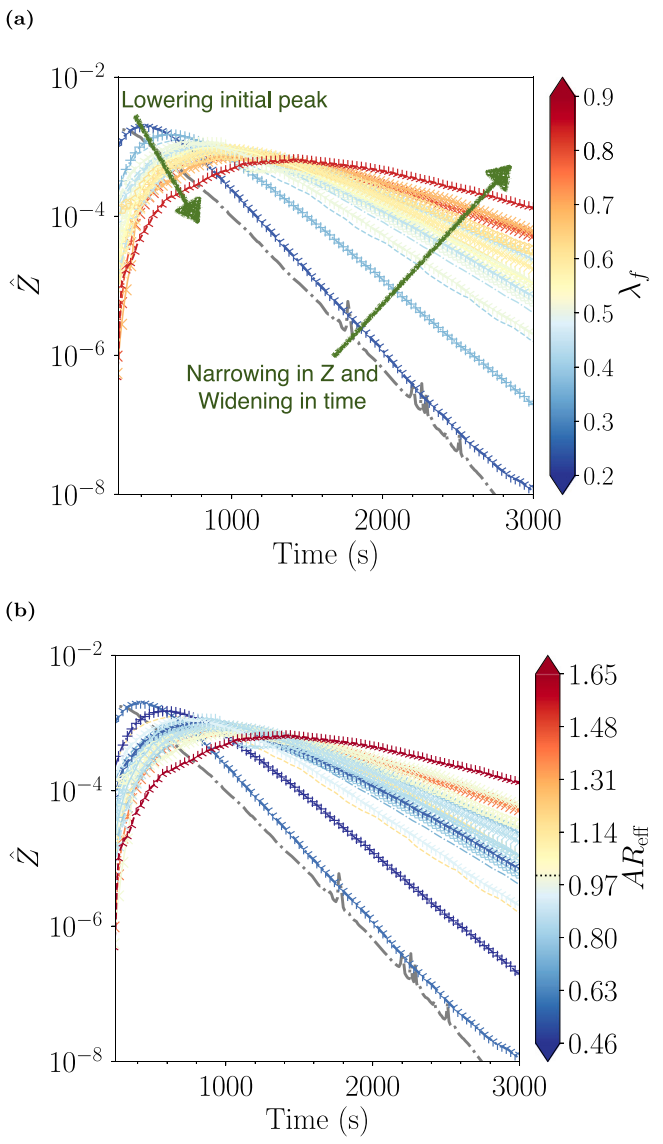

Fig. 13. Age spectra shaded by (a) λ_f; (b) AR_{eff}. The spatial average is taken over $z/H_{\text{ave}} = [0, 1]$. The early-stage time history of the spectra for $t \lesssim 250s$ has been clipped for clarity. For reference, the dash-dotted line coloured in grey plots $\hat{Z}$ for an idealised 3D building array as in Duan and Ngan [7], for which $\lambda_f = 0.25$ and $AR_{\text{eff}} = 1.0$ (indicated by a dotted line on the colour map).

feature of an urban district that may affect the ventilation routes should be reflected in the tracer age distribution.

Fig. 13(a) plots the spatially averaged age spectra, $\hat{Z}$, for different λ_f. It can be seen that $\hat{Z}$ peaks at earlier times (with higher probability) for smaller λ_f, implying that the pollutant scalar reaches a receptor more quickly when λ_f is small, and hence small MTA and improved ventilation can be expected. After the initial transition, the spectra exhibit a stable exponential decay in time, which coincides with the decay behaviour for an idealised 2D urban canyon [16] and a 3D building array [58].

It is also found that there is a clear monotonic dependence of the decay rate (reciprocal of the decay slop) on λ_f. The decay slope is more shallower for large λ_f, implying that ventilation occurs on a much broader range of timescales. As a consequence, the characteristic timescales of ventilation (viz. the residence time analysed in Section 3.1 and the mean tracer age discussed in Section 3.2) increase with λ_f.

The narrowing of the $\hat{Z}$ range (along y-axis) progressively towards higher values and the contemporarily lowering initial peak as λ_f is increased indicate increasing probability of long-timescale excursions of the pollutant tracer and decreasing probability of ventilation occurring on short times. For the latter, the pathways whereby ventilation occurs more rapidly are limited. This explains why ventilation deteriorates (corresponding to large τ in Section 3.1 and high $\hat{\tau}_a$ in Section 3.2) for increased λ_f and improves for decreased λ_f. Similar results are not observed for the other morphometric indices, except for H_{ave}, which is proportionally involved in the definition of λ_f.

By contrast, the dependence of $\hat{Z}$ on the effective canyon aspect ratio presented in Fig. 13(b) looks much less conclusive.

For comparison, results for a 3D array of aligned building cuboids of $\lambda_f = 0.25$ and $AR = 1.0$ (as the building array considered in Duan and Ngan [7]) are indicated in Fig. 13. The slope of $\hat{Z}$ for the idealised case is reasonably close to that for the real urban district at $\lambda_f = 0.2$ (panel a); however, the slope is more steeper than that for the real urban district at $AR_{\text{eff}} \sim 1.0$ (panel b), implying much shorter ventilation timescales in idealised urban topography setups of equivalent canyon aspect ratios to AR_{eff}. This result agrees with Nakayama et al. [67], wherein turbulence statistics inside idealised urban canyons were shown to weaken when the building height inhomogeneity was

increased (namely becoming less idealised in the topography). Departures of the spectra for realistic urban districts from that for the building array case reflect the nonlinear effects that are not captured in idealised urban setups. A thorough comparison of age spectra for idealised building arrays of various canyon aspect ratios with nominal domains of equivalent AR_{eff} may represent an interesting aspect worth exploring in future work.

4. Summary and conclusions

The current study explored the connection between ventilation and urban morphometric indices. The decay of the mean concentrations was found to slow down progressively towards higher λ_f and the retention time, τ_r, exhibited a strong linear scaling with λ_f (R^2 is as high as 0.76). Similar relationship was revealed for the mean tracer age, τ_a, versus λ_f ($R^2 = 0.80$). In addition to the conventional morphometric indices, an effective canyon aspect ratio, AR_{eff}, was proposed, which enables the quantification of the ventilation characteristics with AR_{eff} for realistic urban districts in a manner as that for idealised canyons.

The eddy turnover time, which roughly quantifies the time required for a pollutant scalar to be swept from the ground to the roof-level open boundary, showed a notable monotonic dependence on AR_{eff}, implying the existence of a similar connection between ventilation and AR_{eff}. A conclusive relationship was confirmed for the characteristic ventilation timescales (the retention time, τ_r, and the mean tracer age, τ_a) versus AR_{eff}. Results for urban districts with exceptionally tall buildings ($H_{\max}/H_{\mathrm{ave}} \sim 7$) or areas filled with a substantial portion of irregularly-shaped buildings exhibited large departures with respect to the regressed curves. Nevertheless, the R^2 for the quadratic regression of τ_r versus AR_{eff} and τ_a versus AR_{eff} is up to 0.59 and 0.70, respectively. Further analyses were performed for the tracer age spectra against λ_f and AR_{eff}. A clear progressive change of the spectra with λ_f was observed. The results were compared with that for an aligned building array of unity aspect ratio and $\lambda_f = 0.25$; however, large discrepancies were seen in the comparison for $AR_{\mathrm{eff}} = 1$, which is likely attributed to nonlinear effects that are not well captured in idealised urban topography setups.

Although the building-height variability (σ_H) has been believed to have a strong influence on outdoor ventilation (Cui et al. [14]), we found inconclusive connection between the ventilation timescales and σ_H, which coincides with the results for idealised canyon setups (Lo and Ngan [16]). An unambiguous dependence was not identified neither for the ventilation statistics versus the other morphometric indices, e.g. λ_p and $H_{\max}$, except for H_{ave}, which is proportionally involved in the definition of λ_f. However, it is plausible that the urban canopy height in place of $H_{\max}$, which is dynamically modified by skyscrapers, may exhibit a more conclusive influence on the ventilation (Cheng and Yang [66]).

The results may serve as a useful reference for ventilation parameterisation for realistic urban districts. Urban layout design can take advantage of the study for achieving optimum urban ventilation capability. The identified scaling of the characteristic ventilation timescales with urban morphometric indices can be of particular importance for emergency response against releases of hazardous pollutants in urban areas of complex building geometrical profiles.

A few aspects of theoretical and practical concerns may be worthy of further efforts. The practical one is if the results would hold when trees are present, wherein deposition and additional drag exerted on the canyon flow are non-negligible (cf. Buccolieri et al. [68] and Barbano et al. [69]. Another concern is if thermal effects would alter the identified relationship between ventilation and the morphometric indices, especially for unstably-stratified situations, wherein pollutants driven towards higher vertical levels may quickly decouple from perturbations of the surface roughness obstacles (cf. Kanda and Yamao [60] and Duan and Ngan [7]). It is well known that distinct flow regimes have been classified with respect to the canyon aspect ratio for idealised canyons [8], and various ventilation scenarios extensively investigated (e.g. Cheng et al. [56] and Murena et al. [63]). With the proposed effective canyon aspect ratio, AR_{eff}, to what extent results for idealised canyons can be generalised to real urban districts and the role of nonlinear effects that is not fully reflected in idealised setups may be quantified in future work.

CRediT authorship contribution statement

G. Duan: Writing – original draft, Methodology, Funding acquisition, Formal analysis, Conceptualization. **K. Nakamae:** Visualization, Methodology. **T. Takemi:** Writing – review & editing, Funding acquisition, Methodology.

Declaration of competing interest

The authors declare that they have no known competing financial interests or personal relationships that could have appeared to influence the work reported in this paper.

Data availability

Data will be made available on request.

Acknowledgements

The project was supported by the Natural Science Foundation of Liaoning Province of China (2022-KF-18-07) (Key Program for Science and Technology Innovation) and the Fundamental Research Funds for the Central Universities, China (3132022135). The authors also acknowledge the financial support of the Environment Research and Technology Development Fund of the Environmental Restoration and Conservation Agency (ERCA) of Japan (JPMEERF20192005) and the Japan Society for the Promotion of Science (JSPS) Scientific Research (21H01591).

References

[1] United Nations, World Urbanization Prospects, The 2018 Revision, Department of Economic and Social Affairs, United Nations, 2018.
[2] Y. Li, J. Zhang, D.J. Sailor, G.A. Ban-Weiss, Effects of urbanization on regional meteorology and air quality in Southern California, Atmos. Chem. Phys. 19 (7) (2019) 4439–4457, http://dx.doi.org/10.5194/acp-19-4439-2019.
[3] L. Liang, P. Gong, Urban and air pollution: a multi-city study of long-term effects of urban landscape patterns on air quality trends, Sci. Rep. 10 (1) (2020) 18618, http://dx.doi.org/10.1038/s41598-020-74524-9.
[4] I. Lee, H. Park, Parameterization of the pollutant transport and dispersion in urban street canyons, Atmos. Environ. 28 (14) (1994) 2343–2349, http://dx.doi.org/10.1016/1352-2310(94)90488-X.
[5] V.B.L. Boppana, Z.-T. Xie, I.P. Castro, Large-eddy simulation of dispersion from surface sources in arrays of obstacles, Bound.-Lay. Meteorol. 135 (3) (2010) 433–454, http://dx.doi.org/10.1007/s10546-010-9489-9.
[6] S. Branford, O. Coceal, T.G. Thomas, S.E. Belcher, Dispersion of a point-source release of a passive scalar through an urban-like array for different wind directions, Bound.-Lay. Meteorol. 139 (3) (2011) 367–394, http://dx.doi.org/10.1007/s10546-011-9589-1.
[7] G. Duan, K. Ngan, Influence of thermal stability on the ventilation of a 3-D building array, Build. Environ. 183 (2020) 106969, http://dx.doi.org/10.1016/j.buildenv.2020.106969.
[8] T. Oke, Street design and urban canopy layer climate, Energy Build. 11 (1) (1988) 103–113, http://dx.doi.org/10.1016/0378-7788(88)90026-6.
[9] L. Hunter, G. Johnson, I. Watson, An investigation of three-dimensional characteristics of flow regimes within the urban canyon, Atmos. Environ. 26 (4) (1992) 425–432, http://dx.doi.org/10.1016/0957-1272(92)90049-X.
[10] K. Ngan, K.W. Lo, Revisiting the flow regimes for urban street canyons using the numerical Green's function, Environ. Fluid Mech. 16 (2) (2016) 313–334, http://dx.doi.org/10.1007/s10652-015-9422-3.
[11] J.-F. Sini, S. Anquetin, P.G. Mestayer, Pollutant dispersion and thermal effects in urban street canyons, Atmos. Environ. 30 (15) (1996) 2659–2677.
[12] D. Hertwig, G. Patnaik, B. Leitl, LES validation of urban flow, part II: eddy statistics and flow structures, Environ. Fluid Mech. 17 (3) (2017) 551–578, http://dx.doi.org/10.1007/s10652-016-9504-x.

[13] B. Addepalli, E.R. Pardyjak, Investigation of the flow structure in step-up street canyons-mean flow and turbulence statistics, Bound.-Lay. Meteorol. 148 (1) (2013) 133–155, http://dx.doi.org/10.1007/s10546-013-9810-5.

[14] D. Cui, X. Li, J. Liu, L. Yuan, C.M. Mak, Y. Fan, K. Kwok, Effects of building layouts and envelope features on wind flow and pollutant exposure in height-asymmetric street canyons, Build. Environ. 205 (2021) 108177, http://dx.doi.org/10.1016/j.buildenv.2021.108177.

[15] Z.-L. Gu, Y.-W. Zhang, Y. Cheng, S.-C. Lee, Effect of uneven building layout on air flow and pollutant dispersion in non-uniform street canyons, Build. Environ. 46 (12) (2011) 2657–2665, http://dx.doi.org/10.1016/j.buildenv.2011.06.028.

[16] K.W. Lo, K. Ngan, Characterising the pollutant ventilation characteristics of street canyons using the tracer age and age spectrum, Atmos. Environ. 122 (2015) 611–621, http://dx.doi.org/10.1016/j.atmosenv.2015.10.023.

[17] M. Coburn, Z.-T. Xie, S.J. Herring, Numerical simulations of boundary-layer airflow over pitched-roof buildings, Bound.-Lay. Meteorol. 185 (3) (2022) 415–442, http://dx.doi.org/10.1007/s10546-022-00738-1.

[18] H. Wang, P. Brimblecombe, K. Ngan, Particulate matter inside and around elevated walkways, Sci. Total Environ. (2019) 134256, http://dx.doi.org/10.1016/j.scitotenv.2019.134256.

[19] G. Duan, P. Brimblecombe, Y. Chu, K. Ngan, Turbulent flow and dispersion inside and around elevated walkways, Build. Environ. 173 (2020) 106711, http://dx.doi.org/10.1016/j.buildenv.2020.106711.

[20] L.C. da Silveira, A.P. de Oliveira, M.P. Sánchez, G. Codato, M.J. Ferreira, E.P. Marques Filho, M.Z. Božnar, P. Mlakar, Observational investigation of the statistical properties of surface-layer turbulence in a Suburban area of São Paulo, Brazil: Objective analysis of scaling-parameter accuracy and uncertainties, Bound.-Lay. Meteorol. 185 (2) (2022) 161–195, http://dx.doi.org/10.1007/s10546-022-00726-5.

[21] C.S.B. Grimmond, T.R. Oke, Aerodynamic properties of urban areas derived from analysis of surface form, J. Appl. Meteorol. 38 (9) (1999) 1262–1292, http://dx.doi.org/10.1175/1520-0450(1999)038<1262:APOUAD>2.0.CO;2.

[22] Q. Li, G. Katul, Bridging the urban canopy sublayer to aerodynamic parameters of the atmospheric surface layer, Bound.-Lay. Meteorol. 185 (1) (2022) 35–61, http://dx.doi.org/10.1007/s10546-022-00723-8.

[23] T. Takemi, T. Yoshida, M. Horiguchi, W. Vanderbauwhede, Large-eddy-simulation analysis of airflows and strong wind hazards in urban areas, Urban Clim. 32 (2020) 100625, http://dx.doi.org/10.1016/j.uclim.2020.100625.

[24] G. Duan, T. Takemi, Gustiness in thermally-stratified urban turbulent boundary-layer flows and the influence of surface roughness, J. Wind Eng. Ind. Aerodyn. 208 (2021) 104442, http://dx.doi.org/10.1016/j.jweia.2020.104442.

[25] G. Duan, T. Takemi, Predicting urban surface roughness aerodynamic parameters using random forest, J. Appl. Meteorol. Climatol. 60 (7) (2021) 999–1018, http://dx.doi.org/10.1175/JAMC-D-20-0266.1.

[26] M. Kanda, A. Inagaki, T. Miyamoto, M. Gryschka, S. Raasch, A new aerodynamic parametrization for real urban surfaces, Bound.-Lay. Meteorol. 148 (2) (2013) 357–377, http://dx.doi.org/10.1007/s10546-013-9818-x.

[27] Y. Liu, C.-H. Liu, G.P. Brasseur, C.Y. Chao, Wavelet analysis of the atmospheric flows over real urban morphology, Sci. Total Environ. (2022) 160209, http://dx.doi.org/10.1016/j.scitotenv.2022.160209.

[28] C. Ratti, S. Di Sabatino, R. Britter, M. Brown, F. Caton, S. Burian, Analysis of 3-D urban databases with respect to pollution dispersion for a number of European and American cities, Water Air and Soil Pollut.: Focus 2 (5) (2002) 459–469.

[29] M.R. Raupach, Drag and drag partition on rough surfaces, Bound.-Lay. Meteorol. 60 (4) (1992) 375–395, http://dx.doi.org/10.1007/BF00155203.

[30] B. Maronga, S. Banzhaf, C. Burmeister, T. Esch, R. Forkel, D. Fröhlich, V. Fuka, K.F. Gehrke, J. Geletič, S. Giersch, T. Gronemeier, G. Groß, W. Heldens, A. Hellsten, F. Hoffmann, A. Inagaki, E. Kadasch, F. Kanani-Sühring, K. Ketelsen, B.A. Khan, C. Knigge, H. Knoop, P. Krč, M. Kurppa, H. Maamari, A. Matzarakis, M. Mauder, M. Pallasch, D. Pavlik, J. Pfafferott, J. Resler, S. Rissmann, E. Russo, M. Salim, M. Schrempf, J. Schwenkel, G. Seckmeyer, S. Schubert, M. Sühring, R. von Tils, L. Vollmer, S. Ward, B. Witha, H. Wurps, J. Zeidler, S. Raasch, Overview of the PALM model system 6.0, Geosci. Model Dev. 13 (3) (2020) 1335–1372, http://dx.doi.org/10.5194/gmd-13-1335-2020.

[31] S. Raasch, M. Schröter, PALM-a large-eddy simulation model performing on massively parallel computers, Meteorol. Z. 10 (5) (2001) 363–372.

[32] G. Duan, J.G. Jackson, K. Ngan, Scalar mixing in an urban canyon, Environ. Fluid Mech. 19 (4) (2019) 911–939, http://dx.doi.org/10.1007/s10652-019-09690-0.

[33] T. Yoshida, T. Takemi, M. Horiguchi, Large-eddy-simulation study of the effects of building-height variability on turbulent flows over an Actual Urban Area, Bound.-Lay. Meteorol. 168 (1) (2018) 127–153.

[34] S.-B. Park, J.-J. Baik, S.-H. Lee, Impacts of mesoscale wind on turbulent flow and ventilation in a densely built-up urban area, in: Journal of Applied Meteorology and Climatology, J. Appl. Meteorol. Climatol. 54 (4) (2015) 811–824, http://dx.doi.org/10.1175/JAMC-D-14-0044.1.

[35] K.W. Lo, K. Ngan, Characterizing ventilation and exposure in street canyons using Lagrangian particles, J. Appl. Meteorol. Climatol. 56 (5) (2017) 1177–1194, http://dx.doi.org/10.1175/JAMC-D-16-0168.1.

[36] E. Furtak-Cole, K. Ngan, Predicting mean velocity profiles inside urban canyons, J. Wind Eng. Ind. Aerodyn. 207 (2020) 104280, http://dx.doi.org/10.1016/j.jweia.2020.104280.

[37] T.S. Lund, X. Wu, K.D. Squires, Generation of turbulent inflow data for spatially-developing boundary layer simulations, J. Comput. Phys. 140 (2) (1998) 233–258.

[38] H. Kataoka, M. Mizuno, Numerical flow computation around aeroelastic 3D square cylinder using inflow turbulence, Wind Struct. 5 (2002) 379–392, http://dx.doi.org/10.12989/was.2002.5.2_3_4.379.

[39] D. Hertwig, G. Patnaik, B. Leitl, LES validation of urban flow, part I: flow statistics and frequency distributions, Environ. Fluid Mech. 17 (3) (2017) 521–550, http://dx.doi.org/10.1007/s10652-016-9507-7.

[40] M. Horiguchi, K. Tatsumi, A.-P. Poulidis, T. Yoshida, T. Takemi, Large-scale turbulence structures in the atmospheric boundary layer observed above the suburbs of Kyoto City, Japan, Bound.-Lay. Meteorol. 184 (2) (2022) 333–354, http://dx.doi.org/10.1007/s10546-022-00707-8.

[41] A.S. Monin, A. Obukhov, Basic laws of turbulent mixing in the surface layer of the atmosphere, Contrib. Geophys. Inst. Acad. Sci. USSR 151 (1954) 163–187, Monin1954.

[42] J.W. Deardorff, Stratocumulus-capped mixed layers derived from a three-dimensional model, Bound.-Lay. Meteorol. 18 (4) (1980) 495–527.

[43] M. Belda, J. Resler, J. Geletič, P. Krč, B. Maronga, M. Sühring, M. Kurppa, F. Kanani-Sühring, V. Fuka, K. Eben, N. Benešová, M. Auvinen, Sensitivity analysis of the PALM model system 6.0 in the urban environment, Geosci. Model Dev. Discuss. 2020 (2020) 1–32, http://dx.doi.org/10.5194/gmd-2020-126.

[44] D. Muñoz-Esparza, B. Kosović, C. García-Sánchez, J. van Beeck, Nesting turbulence in an offshore convective boundary layer using large-eddy simulations, Bound.-Lay. Meteorol. 151 (3) (2014) 453–478, http://dx.doi.org/10.1007/s10546-014-9911-9.

[45] J.H. Williamson, Low-storage Runge-Kutta schemes, J. Comput. Phys. 35 (1) (1980) 48–56.

[46] L.J. Wicker, W.C. Skamarock, Time-splitting methods for elastic models using forward time schemes, in: Monthly Weather Review, Mon. Weather Rev. 130 (8) (2002) 2088–2097, http://dx.doi.org/10.1175/1520-0493(2002)130<2088:TSMFEM>2.0.CO;2.

[47] A.A.N. Patrinos, A.L. Kistler, A numerical study of the Chicago lake breeze, Bound.-Lay. Meteorol. 12 (1) (1977) 93–123, http://dx.doi.org/10.1007/BF00116400.

[48] B. Maronga, M. Gryschka, R. Heinze, F. Hoffmann, F. Kanani-Sühring, M. Keck, K. Ketelsen, M.O. Letzel, M. Sühring, S. Raasch, The parallelized large-eddy simulation model (PALM) version 4.0 for atmospheric and oceanic flows: model formulation, recent developments, and future perspectives, Geosci. Model Dev. 8 (8) (2015) 2515–2551, http://dx.doi.org/10.5194/gmd-8-2515-2015.

[49] W.C. Cheng, C.-H. Liu, Large-eddy simulation of flow and pollutant transports in and above two-dimensional idealized street canyons, Bound.-Lay. Meteorol. 139 (3) (2011) 411–437, http://dx.doi.org/10.1007/s10546-010-9584-y.

[50] K.W. Lo, K. Ngan, Predictability of turbulent flow in street canyons, Bound.-Lay. Meteorol. 156 (2) (2015) 191–210, http://dx.doi.org/10.1007/s10546-015-0014-z.

[51] G. Duan, K. Ngan, Effects of time-dependent inflow perturbations on turbulent flow in a street canyon, Bound.-Lay. Meteorol. 167 (2) (2018) 257–284, http://dx.doi.org/10.1007/s10546-017-0327-1.

[52] T. Gronemeier, K. Surm, F. Harms, B. Leitl, B. Maronga, S. Raasch, Validation of the dynamic core of the PALM model system 6.0 in urban environments: LES and wind-tunnel experiments, Geosci. Model Dev. Discuss. 2020 (2020) 1–26, http://dx.doi.org/10.5194/gmd-2020-172.

[53] M. Pavageau, M. Schatzmann, Wind tunnel measurements of concentration fluctuations in an urban street canyon, Atmos. Environ. 33 (1999) 3961–3971, http://dx.doi.org/10.1016/S1352-2310(99)00138-7.

[54] C.-H. Liu, M.C. Barth, Large-eddy simulation of flow and scalar transport in a modeled street canyon, J. Appl. Meteorol. 41 (6) (2002) 660–673.

[55] M. Holzer, T.M. Hall, Transit-time and tracer-age distributions in geophysical flows, J. Atmos. Sci. 57 (21) (2000) 3539–3558.

[56] W.C. Cheng, C.-H. Liu, D.Y.C. Leung, Computational formulation for the evaluation of street canyon ventilation and pollutant removal performance, Atmos. Environ. 42 (40) (2008) 9041–9051, http://dx.doi.org/10.1016/j.atmosenv.2008.09.045.

[57] J. Hang, M. Sandberg, Y. Li, Age of air and air exchange efficiency in idealized city models, Build. Environ. 44 (8) (2009) 1714–1723, http://dx.doi.org/10.1016/j.buildenv.2008.11.013.

[58] G. Lau, K. Ngan, Analysing urban ventilation in building arrays with the age spectrum and mean age of pollutants, Build. Environ. 131 (2018) 288–305, http://dx.doi.org/10.1016/j.buildenv.2018.01.010.

[59] F.T. DePaul, C.M. Sheih, A tracer study of dispersion in an urban street canyon, Atmos. Environ. (1967) 19 (4) (1985) 555–559, http://dx.doi.org/10.1016/0004-6981(85)90034-4.

[60] I. Kanda, Y. Yamao, Passive scalar diffusion in and above urban-like roughness under weakly stable and unstable thermal stratification conditions, J. Wind Eng. Ind. Aerodyn. 148 (2016) 18–33, URL: http://www.sciencedirect.com/science/article/pii/S0167610515002573.

[61] K. Ngan, K.W. Lo, Linear error dynamics for turbulent flow in urban street canyons, J. Appl. Meteorol. Climatol. 56 (5) (2017) 1195–1208, http://dx.doi.org/10.1175/JAMC-D-16-0173.1.

[62] W. Anderson, Q. Li, E. Bou-Zeid, Numerical simulation of flow over urban-like topographies and evaluation of turbulence temporal attributes, J. Turbul. 16 (9) (2015) 809–831, http://dx.doi.org/10.1080/14685248.2015.1031241.

[63] F. Murena, A. Di Benedetto, M. D'Onofrio, G. Vitiello, Mass transfer velocity and momentum vertical exchange in simulated deep street canyons, Bound.-Lay. Meteorol. 140 (1) (2011) 125–142.

[64] L. Yao, C.-H. Liu, Z. Mo, W.-C. Cheng, G.P. Brasseur, C.Y. Chao, Statistical analysis of the organized turbulence structure in the inertial and roughness sublayers over real urban area by building-resolved large-eddy simulation, Build. Environ. (2021) 108464, http://dx.doi.org/10.1016/j.buildenv.2021.108464.

[65] B.S. Sützl, G.G. Rooney, M. van Reeuwijk, Drag distribution in idealized heterogeneous urban environments, Bound.-Lay. Meteorol. 178 (2) (2021) 225–248, http://dx.doi.org/10.1007/s10546-020-00567-0.

[66] W.-C. Cheng, Y. Yang, Scaling of flows over realistic urban geometries: A large-eddy simulation study, Bound.-Lay. Meteorol. (2022) http://dx.doi.org/10.1007/s10546-022-00749-y.

[67] H. Nakayama, T. Takemi, H. Nagai, LES analysis of the aerodynamic surface properties for turbulent flows over building arrays with various geometries, J. Appl. Meteorol. Climatol. 50 (8) (2011) 1692–1712, http://dx.doi.org/10.1175/2011JAMC2567.1.

[68] R. Buccolieri, S.M. Salim, L.S. Leo, S.D. Sabatino, A. Chan, P. Ielpo, G. de Gennaro, C. Gromke, Analysis of local scale tree-atmosphere interaction on pollutant concentration in idealized street canyons and application to a real urban junction, Atmos. Environ. 45 (9) (2011) 1702–1713, http://dx.doi.org/10.1016/j.atmosenv.2010.12.058.

[69] F. Barbano, S. Di Sabatino, R. Stoll, E.R. Pardyjak, A numerical study of the impact of vegetation on mean and turbulence fields in a European-city neighbourhood, Build. Environ. 186 (2020) 107293, http://dx.doi.org/10.1016/j.buildenv.2020.107293.